

Resonant magnetic x-ray scattering in a series of uranium compounds

C. C. Tang and W. G. Stirling*

Physics Department, School of Physical Science and Engineering, University of Keele, Keele, Staffordshire ST5 5BG, United Kingdom

G. H. Lander

Commission of the European Communities, Joint Research Centre, Institute for Transuranium Elements, Postfach 2340, 7500 Karlsruhe, Federal Republic of Germany

Doon Gibbs and W. Herzog†

Physics Department, Brookhaven National Laboratory, Upton, New York 11973

Paolo Carra and B. T. Thole‡

European Synchrotron Radiation Facility, Boîte Postale 220, F-38043 Grenoble, France

K. Mattenberger and O. Vogt

Laboratorium für Festkörperphysik, Eidgenössische Technische Hochschule, CH-8093 Zürich, Switzerland

(Received 7 May 1992)

We report results of x-ray scattering experiments on the antiferromagnetic uranium compounds UO_2 , USb , and $(\text{U}_{0.85}\text{Th}_{0.15})\text{Sb}$. The energy dependence of the x-ray scattering cross section is reported in the range 3.5–3.9 keV, which includes the M_{IV} and M_{V} absorption edges. The energy dependencies are very similar and well represented by atomic-resonance methodology. Differences occur in the ratio of intensities (branching ratio) of the two absorption edges, which are larger in UO_2 than in the other materials. *Ab initio* calculations based on atomic physics suggest that such differences may arise from differing $5f$ -electron configurations. Unfortunately, we have not measured accurately the absorption coefficient over the two edges, so that our corrections to the intensities must be regarded as qualitative. This prevents a quantitative comparison between the observed and calculated branching ratios. Consistent with the calculated cross section, the magnetic scattering of the σ -polarized incident beam is rotated to π polarization. No unusual effects were found at the M_{IV} edge of Th in the pseudobinary compound.

I. INTRODUCTION

The advent of high-intensity x-ray synchrotron sources has meant that direct-x-ray studies of magnetic phenomena have now become possible, thus providing a complementary probe to more conventional neutron-scattering studies.¹ For our present purposes there are two aspects of the x-ray cross section that are of interest. The first is the possibility of using x-ray scattering to separate the spin and orbital components of the total magnetization.² This separation is of particular interest in actinide ($5f$) compounds, such as those studied here, as the exact electronic ground state remains uncertain, and there are definitive predictions of the spin and orbital components from band-structure calculations.³ However, the exploitation of this aspect of the x-ray cross section has proved difficult. The x-ray scattering from magnetically ordered moments is already weak,² and the systems in which the separation of spin and orbital moments is of interest usually have small total moments, thus leading to very small x-ray intensities. An attempt to separate the components was performed in metallic holmium,⁴ in which L and S are large, and, more recently in the actinide compound UAs ,⁵ but in both cases the results were qualitative. These kinds of measurements will certainly benefit from more intense x-ray beams, such as those envisaged from

the new generation of insertion devices.

The second aspect of the x-ray cross section that is of interest is its energy dependence near atomic-absorption edges. At these energies Hannon *et al.*⁶ have shown that off-resonance magnetic scattering may be overwhelmed by additional resonant-magnetic contributions, contained in the anomalous scattering amplitude and ascribed to spin-orbit and exchange interactions.¹ The (virtual) transitions, associated with resonant-magnetic x-ray scattering, have in general an electric multiplet character. In the case of holmium, the resonant effects near the L_{III} edge (8.067 keV) result in an increase in the magnetic-scattering cross section by a factor of about 50.^{1,4} The electric dipole ($E1$) transition at the L_{III} edge in Ho is $2p \rightarrow 5d$, whereas electric quadrupole ($E2$) transitions connect to the $4f$ shell. As pointed out by Hannon *et al.*,⁶ what is required for a very large effect is an $E1$ process involving transitions to a state in which there is an appreciable density of unpaired electrons. For $3d$ transition metals such edges are the L_{II} and L_{III} at energies less than 1 keV. At these energies diffraction effects can be observed only in structures with long repeat units, e.g., multilayers. However, Kao *et al.*⁷ have shown that reflectivity measurements are also sensitive to resonance effects. The situation is more convenient for diffraction in the $5d$ series, where L -edge absorption edges occur

above 10 keV, but there are not many systems with ordered $5d$ electrons. In some recent experiments on a Co-Pt alloy, these effects have been observed at the Pt L_{III} -edge energy.⁸ For f systems the relevant edges are M_{IV} and M_V . For the lanthanides ($4f$) these energies are between 1 and 2 keV, which is again a difficult region for diffraction experiments. (Recall that for x rays $E = 12.398/\lambda$, where E is in keV, λ is in angstroms.) However, the M_{IV} and M_V edges for $5f$ systems are between 3 and 4 keV, so that very large effects should be seen.

Following the enumeration of these conditions by Hannon *et al.*⁶ Isaacs *et al.*¹⁰ performed an experiment on the uranium compound UAs and observed an enhancement of the magnetic signal by many orders of magnitude when the energy was tuned to the M_{IV} edge of 3.728 keV. The magnetic scattering at the M_{IV} edge was reported as $\sim 1\%$ of the charge scattering. At the M_{IV} edge an electron from the filled $3d_{3/2}$ level is promoted to an empty $5f_{5/2}$ state and the intermediate state forms a strong resonance, partly because the $5f$ states are relatively narrow in energy. Given the apparent ease with which this magnetic-resonance scattering can be observed, an important question is, what experiments are worth pursuing at these energies? We cannot easily use these intensities to separate the spin and orbital components of the magnetization, at least not until further theory is forthcoming. Present theories to separate S and L rely on the scattering being nonresonant.²

Hannon *et al.*⁶ have pointed out that both the shape and strength of the resonance may give information on the electronic structure of the material in question. Our primary motivation, therefore, was to examine the effects in a series of uranium materials of different electronic structure. In this paper we describe x-ray experiments on the antiferromagnets UO_2 , USb, and $U_{0.85}Th_{0.15}Sb$.

One interesting aspect is the so-called branching ratio, i.e., the ratio of the amplitudes at the M_{IV} and M_V reso-

nant energies. We describe in Sec. V the *ab initio* calculation of these spectra and compare the branching ratios with those obtained experimentally.

The experimental details are given in Sec. II, the results in Sec. III, the theoretical form of the cross section and results of least-squares fits to the data in Sec. IV, and a discussion in Sec. VI.

II. EXPERIMENTAL DETAILS

All of the experiments described in this paper were performed on the beam line X22C at the National Synchrotron Light Source (NSLS) at Brookhaven National Laboratory. The beam line, which views synchrotron light from a bending magnet located in the 2.5-GeV NSLS storage ring, contains a doubly focusing nickel-coated mirror (spotsize ~ 1 mm²) and a fixed-exit Ge (111) double-crystal monochromator. The available energy range is from ~ 3 to 30 keV. Most of our experiments were performed in the region of 3–4 keV. A serious problem with working at these energies is the strong absorption of the x-ray beam in air or through conventional Be windows. For example, for 3.5-keV x rays, the absorption coefficient for nitrogen is 0.1 cm⁻¹ and a 250- μ m Be window absorbs half the beam. In our experiments we had three Be windows of 250 μ m between the source and detector and four thin Kapton windows, two of each sealing the evaluated chambers between source slits and sample and sample and detector. In addition, air scattering was minimized by surrounding the short air paths around the sample cryostat with helium-filled bags. NaI scintillation detectors were used to count the incident and scattered photons.

The samples used in the present studies were all single crystals, usually in the form of small ($\sim 3 \times 3 \times 0.1$ mm³) plates with a [001] normal to the large face of the crystal. No particular effort was made to clean or etch the crystal surfaces, although in all cases they were reasonably flat

TABLE I. Magnetic characteristics of the uranium samples used in this and related studies. All materials are face-centered cubic. The type-I and -IA structures have (001) planes of parallel moments stacked in sequences $+ - + -$ and $+ + - -$, respectively. \mathbf{q} is the ordering wave vector in all cases in the notation $[0,0,\mathbf{q}]$. Different structures single \mathbf{k} , double \mathbf{k} , etc. refer to number of components coexisting (see Ref. 14). The moment components are perpendicular to \mathbf{q} in UO_2 and parallel in the other materials. All these magnetic structures are discussed in detail in Ref. 14. The magnetic moment is that at 5 K.

Compound	Lattice parameter (Å)	T_N (K)	Magnetic structure at 10 K	Magnetic moment (μ_B)
UO_2	5.470	31	type I triple \mathbf{k} $\mathbf{q} = 1.0 \mu \parallel \mathbf{q}$	1.8
USb	6.191	213	type I triple \mathbf{k} $\mathbf{q} = 1.0 \mu \parallel \mathbf{q}$	2.8
$(U_{0.85}Th_{0.15})Sb$	6.195	~ 190	type IA triple \mathbf{k} $\mathbf{q} = 0.5 \mu \parallel \mathbf{q}$	2.7
UAs	5.779	124	type IA double \mathbf{k} $\mathbf{q} = 0.5 \mu \parallel \mathbf{q}$	2.2
UN	4.890	53	type I single \mathbf{k} $\mathbf{q} = 1.0 \mu \parallel \mathbf{q}$	0.75

and shiny. All reflections were examined in reflection geometry from the (001) face. Because the (001) faces are natural cleavage planes for USb and related compounds with the NaCl structure, these surfaces have an excellent mosaic spread, normally less than 0.05° . The UO_2 crystal, on the other hand, was much broader than this. The crystals were mounted on the cold finger of a standard Displex closed-cycle refrigerator. Normally, a radiation shield encloses the sample, but a large hole was cut in this to prevent further absorption of the beam. The external Be shield with $500\ \mu\text{m}$ thick. All experiments reported in this paper were performed with the sample at $T \sim 12\ \text{K}$, which is well below T_N for all three antiferromagnets. The magnetic characteristics of the samples considered here are given in Table I.

In certain cases it is useful to be able to analyze the linear polarization of the scattered photon beam.¹⁰ The principle of polarization analysis is that, if the scattered beam is further scattered by an angle of $\pi/2$ first in and then out of the plane of scattering (defined by the incident and final wave vectors \mathbf{k} and \mathbf{k}' , respectively, and the momentum transfer \mathbf{K}), the intensities of the σ - and π -polarized components of the scattered beam may be measured independently.^{1,10} The instrument has this capability of performing linear polarization analysis, but it is always necessary to find an analyzer crystal with a plane spacing that gives a Bragg reflection at $2\theta = 90^\circ$ for the energy being used. For the results reported here, Al(111) and LiF(111) reflections were used.

The results for the energy dependence of the magnetic scattering and the degree of linear polarization were derived from integrated intensities. These were obtained by rocking the crystals through the Bragg angle. The background obtained far from the Bragg reflection in these scans may be taken as a measure of the sample fluorescence. This provides an on-line calibration of the x-ray energy as the fluorescence is related to the absorption. The raw data from the (102) reflection in UO_2 are shown in Fig. 1(a). Note a change of scale for lower energies.

The fluorescence spectra measured for each material were used to calibrate the energy scale by comparison with the total-electron-yield spectra obtained for a number of uranium compounds by Kalkowski *et al.*¹¹ The M_V and M_{IV} white-line energies in the experimental fluorescence spectra were fixed at the values taken from the electron-yield experiments.

The corrections for the energy-dependent absorption represent the most difficult part of the data treatment. Since it is extremely difficult to prepare homogeneous foils of the uranium material studied thin enough for direct (transmission) absorption measurements, preliminary corrections were used by converting the measured fluorescence to the absorption coefficient. This was found to be unsatisfactory, as the procedure yielded absorption coefficients in the white-line regions which did not agree sufficiently well with the electron-yield results of Kalkowski *et al.*¹¹ Therefore a function was constructed with arctangent functions describing the tabulated uranium attenuation coefficients below, between, and above the M_V and M_{IV} absorption edges. The rapidly varying uranium white lines were modeled by Lorentzian func-

tions of full width 5 eV, corresponding to the observed width of the fluorescence spectra, and of height adjusted to fit the area of the white-line peaks in the electron-yield data (Fig. 5) of Kalkowski *et al.*¹¹ For the different materials studied, due account was taken of the differing anion-mass-absorption coefficients and the different den-

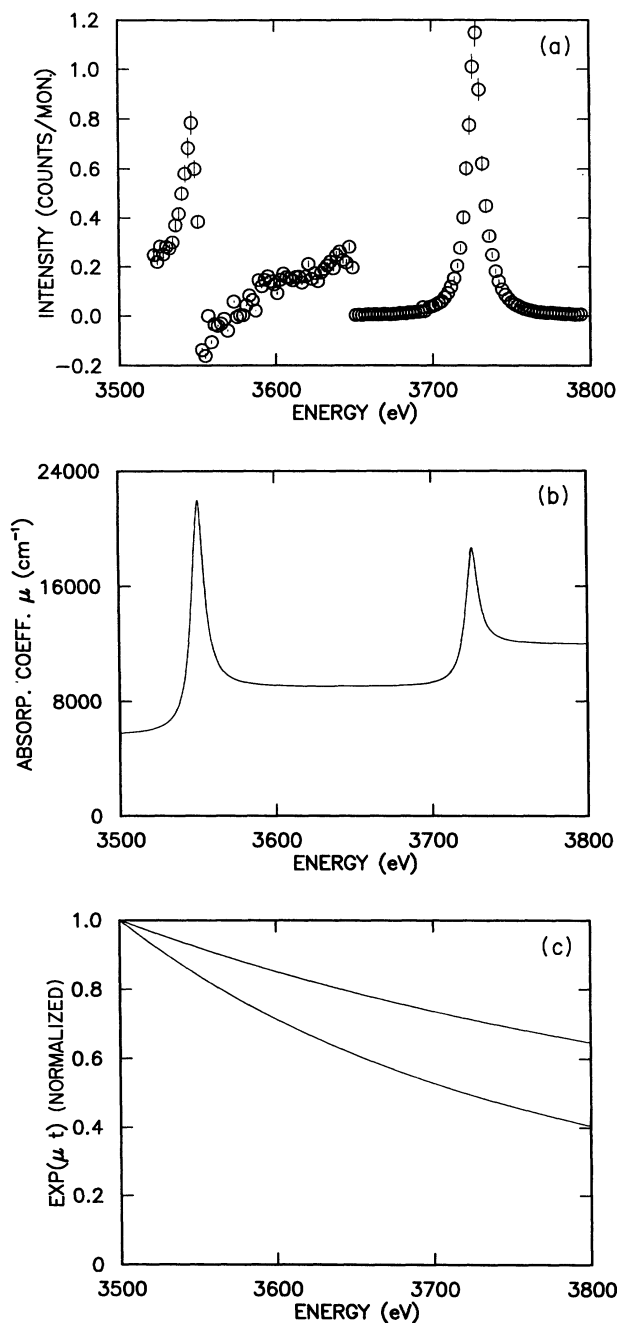


FIG. 1. (a) Data on a linear scale for the $\text{UO}_2(102)$ reflection at 12 K. Note that the low-energy region up to 3.6 keV, which includes the M_V resonance, has been multiplied by a factor of 60. (b) Deduced absorption coefficient as a function of energy for UO_2 . (c) Normalized (at 3.5 keV) absorption coefficients as a function of energy for the Be (upper) and Kapton (lower) windows present in our experiments.

sities. While this procedure yields a line shape which captures important elements of the known electron-yield spectra and of the conditions of our experiment, it does not yield a reliable absorption correction for the data, such as would be obtained from a direct measurement of the absorption through a thin UO_2 foil under the experimental conditions. For this reason we have to treat our experimental results for the branching ratio as qualitative. It is interesting, nonetheless, to use this *ad hoc* absorption correction to find branching ratios and compare them with calculations, and this is done below. An example of the absorption coefficient for UO_2 obtained as outlined above is given in Fig. 1(b); this should be compared with the data of Kalkowski *et al.*¹¹ In the correction procedure, allowance was also made for the effect of the beryllium and Kapton windows in the beam-line components and for the beryllium cryostat tails. The function forms used were $\mu_{\text{Be}} = 1067.9/E^{2.931}$, for a total Be thickness of 750 μm , and $\mu_{\text{Kapton}} = 4567/E^{3.3}$, for a total Kapton thickness of 52 μm , with E in keV. These correction factors were normalized to unity at an energy of 3.5 keV. The energy variation of these factors is shown in Fig. 1(c).

One unusual aspect of the data collection is worth commenting on. In the reciprocal-lattice construction for (001) reflections, the point of intersection of \mathbf{k} and \mathbf{k}' moves along the bisector normal to the reciprocal-lattice vector [001], so that the radius of the Ewald sphere is governed by $2\pi/k$ ($=2\pi/k'$) and the sphere goes through the points (000) and (001). For the geometry used, in which the directions [100] and [010] line in the surface of the crystal, the Ewald sphere may also pass through the point $(\bar{1}02)$ for a certain choice of wavelength. Since both (001) and (102) are allowed, magnetic-reflection multiple-scattering conditions exist at this particular wavelength, leading to possible changes in the intensities. This coincidence condition is, of course, related to the ratio a/λ , where a is the lattice parameter. We have found geometrically that this occurs for $E = 3.56$ keV in UO_2 and 3.18 keV in USb. For UO_2 this energy is close to the M_V edge, and we have found that the intensities were irreproducible near this energy. Since it represents coupling (001)- and (102)-type beams, both intensities might be affected. In each case for UO_2 we have performed an identical experiment at 50 K (above T_N) over the region 3.5–3.6 keV and subtracted it from the low-temperature data. This subtraction is the cause of some of the small negative numbers in the UO_2 plots. Normally, of course, the method to check for multiple scattering is to change λ ; such a procedure is not possible in this case. Another method of verifying these effects is to rotate the sample about the scattering vector, which is difficult in our experiment.

III. RESULTS

We have already seen in Fig. 1 the important changes that occur in magnetic intensity and absorption when the incident photon energy is close to the M_{IV} and M_V resonances. Figure 2 shows the intensity from the $\text{UO}_2(001)$ magnetic reflection on a linear scale at the two edges. Note that these data have not been corrected for absorp-

tion. The latter correction does change the width and intensity of the peak, and may also affect the determination of the position. Figures 3, 4, and 5 show data in a format similar to Fig. 2 for the magnetic reflections from $\text{UO}_2(102)$, USb, and $(\text{U}_{0.85}\text{Th}_{0.15})\text{Sb}$, respectively. The solid lines are fits to the data, which are discussed in the following section.

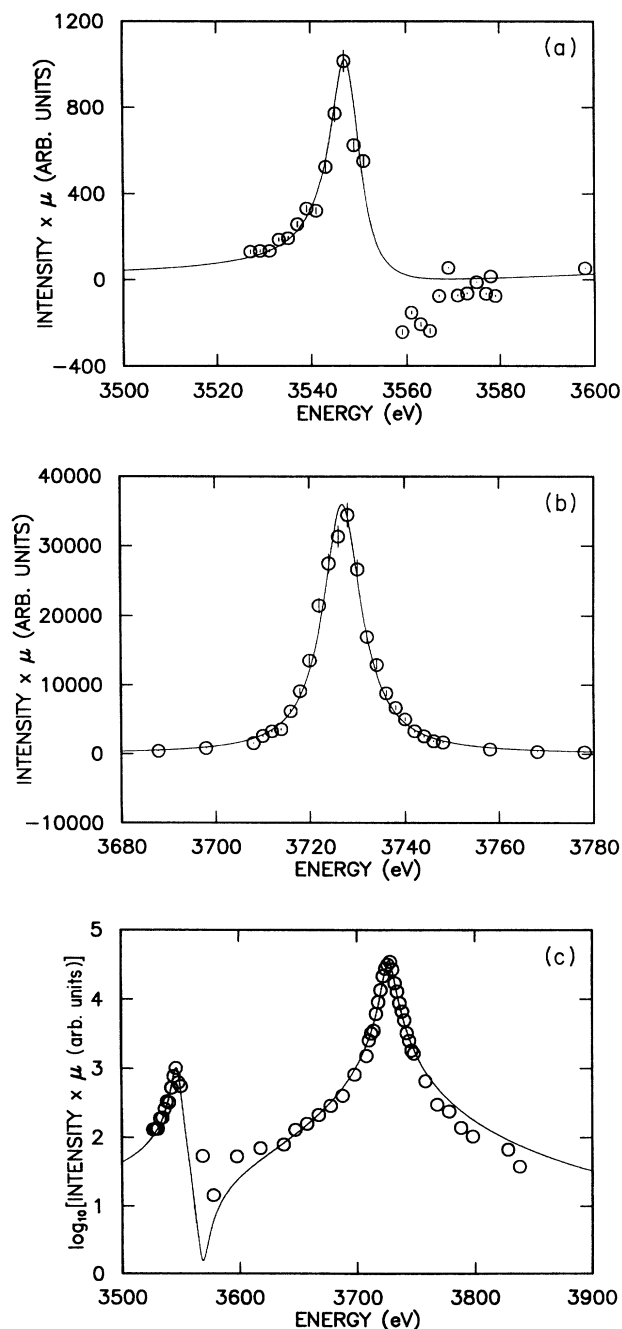


FIG. 2. (a) Energy dependence of the integrated intensity of the (001) magnetic reflection from UO_2 at 12 K for the M_V resonance. The solid line represents the fit to the data as discussed in the text. (b) As in (a) for the M_{IV} resonance. (c) Energy dependence of absorption corrected data for the (001) magnetic reflection from UO_2 at $T = 12$ K. The solid line represents the fit discussed in the text. Note the logarithmic intensity scale.

IV. ANALYSIS

A. Theoretical form of the cross section

Following previous work,⁶ we discuss briefly some general theoretical results obtained for the resonant-magnetic scattering of x rays.

Given a magnetic ion, the amplitude for coherent elastic scattering, in the case of a (virtual) $E1$ transition (in our case $3d \rightarrow 5f$), has the form⁶

$$f_{E1} = \frac{3}{4}\chi\{\hat{e}'^* \cdot \hat{e}(F_{11} + F_{1-1}) - (\hat{e}'^* \times \hat{e}) \cdot \hat{z}_n(F_{11} - F_{1-1}) + (\hat{e}'^* \cdot \hat{z}_n)(\hat{e} \cdot \hat{z}_n)[2F_{10} - F_{11} - F_{1-1}]\}, \quad (1)$$

where \hat{e} and \hat{e}' denote, respectively, incident final polarizations, and \hat{z}_n represents the local quantization axis of the magnetic ion. Also (assuming $T=0$),

$$F_{1,M}(k) = \frac{8\pi}{\chi} k^2 \sum_{\alpha', J'} \frac{|\langle \alpha' J M_J | Q_{1M} | \alpha J M_J \rangle|^2}{E_{\alpha' J'} - E_{\alpha J} - \hbar\omega - i\Gamma/2}, \quad (2)$$

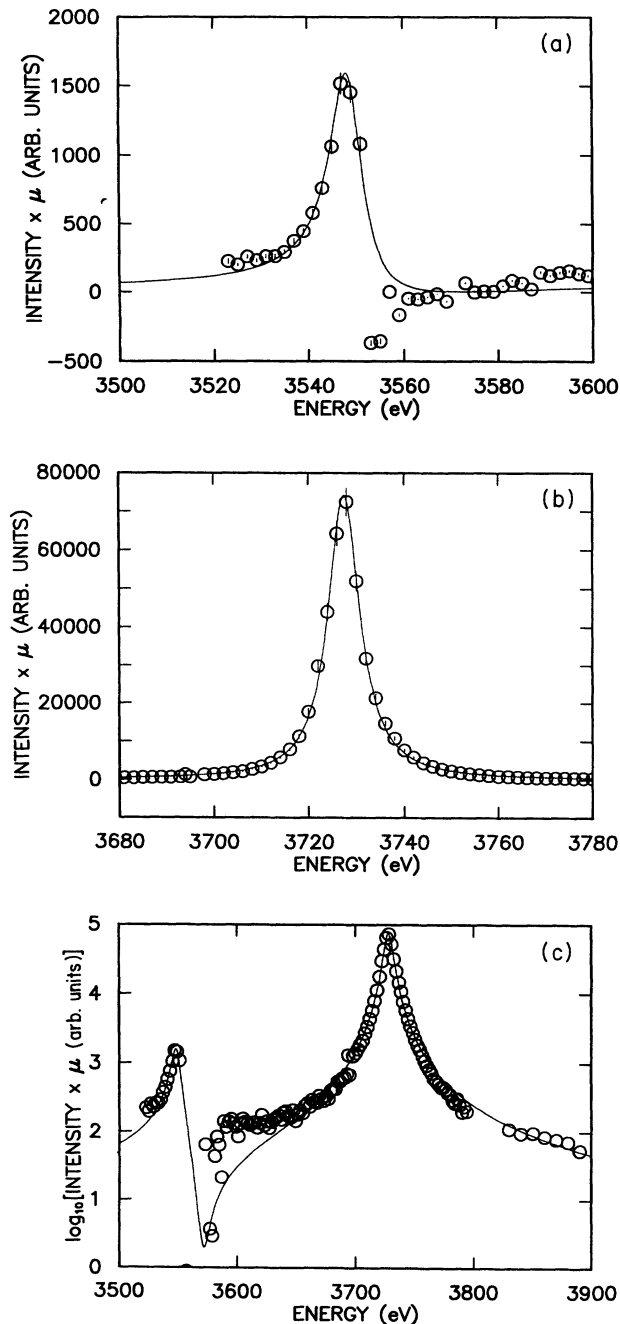


FIG. 3. Data from the $\text{UO}_2(102)$ reflection at 12 K presented in the same format as Fig. 2.

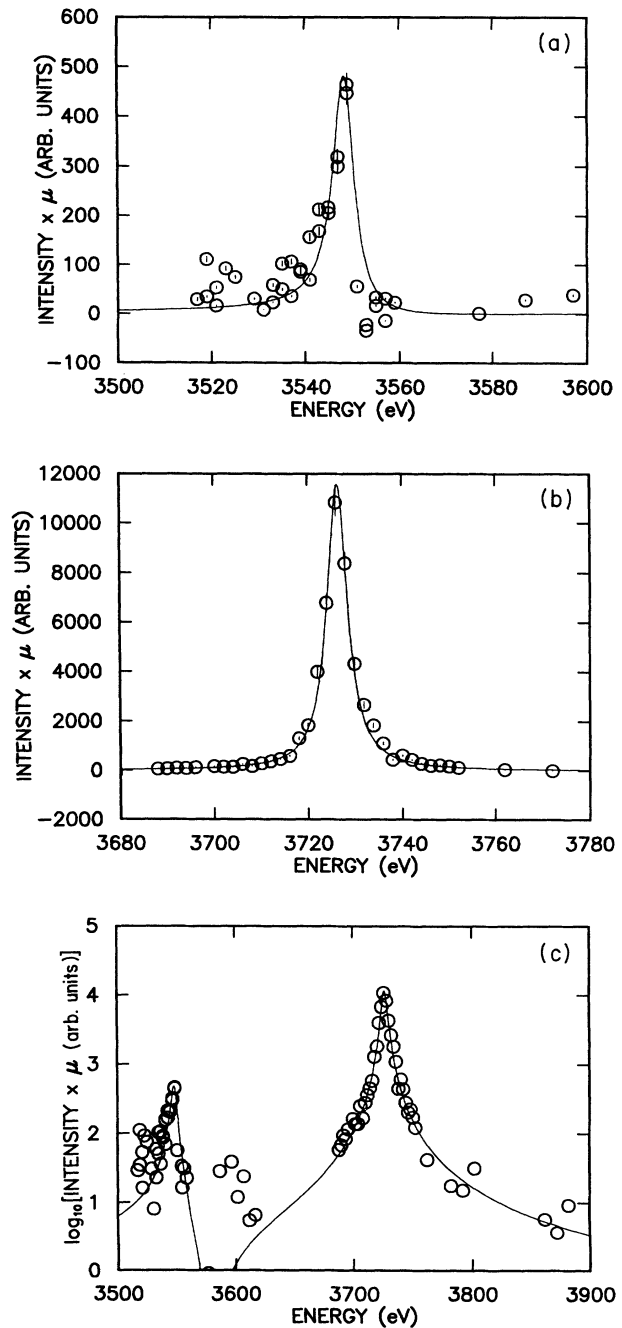


FIG. 4. Data from the $\text{USb}(001)$ magnetic reflection at 12 K presented in the same format as Fig. 2. The negative intensities in (a) arise from the correction for background and reflect the small magnetic intensities at these energies.

with the electric dipole operator given by ($kr \ll 1$)

$$Q_{1M} = -\frac{1}{3}e \sum_j r_j Y_{LM}(\hat{r}_j).$$

Here the index j runs over all electrons of the ion; k represents the photon wave number.

In Eq. (1), derived by neglecting crystal-field effects, the first term describes anomalous charge scattering; the remaining terms, with their \hat{z}_n dependence, bring in sensitivity to the magnetic properties of the system. The

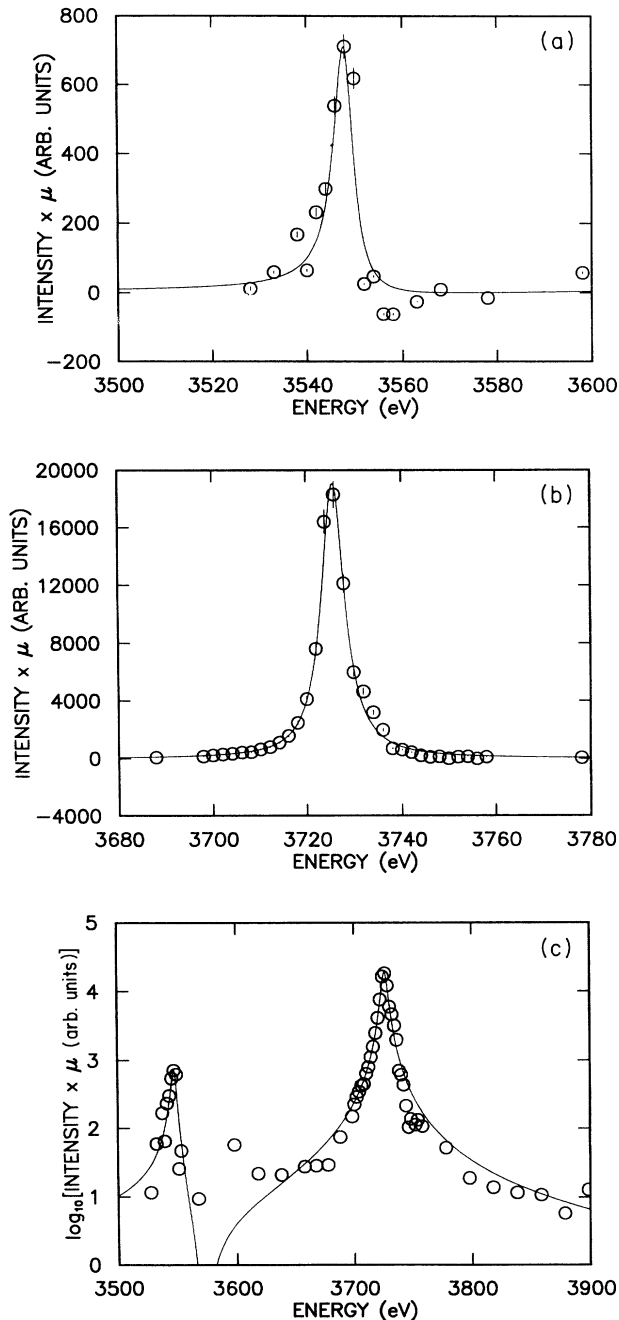


FIG. 5. Data from $U_{0.85}Th_{0.15}Sb(00\frac{5}{2})$ magnetic reflection at 12 K presented in the same format as Figs. 2 and 4.

presence of these magnetic components in the resonant amplitude is ascribed to the combined effect of spin-orbit and exchange interactions.¹²

For measurements in the $\alpha_i \rightarrow \pi_f$ channel, the magnetic signal at \mathbf{q} is controlled by the polarization response $(\hat{e}'^* \times \hat{e}) \cdot \hat{z}_n$. In this case magnetic and charge peaks do not overlap, and there is no interference between magnetic and charge scattering. For $\sigma_i \rightarrow \sigma_f$ or π_f , the response $(\hat{e}'^* \cdot \hat{z}_n)(\hat{e} \cdot \hat{z}_n)$ gives magnetic peaks at $2\mathbf{q}$. In this case magnetic and charge scattering coincide, and the magnetic signal is not detectable with our experimental setup.¹³

The quantities $F_{1,M}(k)$ have appreciable value only near the resonant energies, leading to very sharp changes in intensities in the proximity of the M_{IV} and M_V edges. Both the intensity and energy width (multiplet structure) of the spectra will be sensitive to the electronic structure of the system under consideration. Specifically, they depend on the matrix elements between the initial state $|\alpha JM_J\rangle$ and the final states $|\alpha' J' M_J'\rangle$, under the optical selection rules $\Delta J = 0 \pm 1$. (The label α denotes all the quantum numbers, besides J , which are necessary to specify the atomic state.)

Going over to a 2×2 matrix representation of the amplitude f_{E1} , in the basis of two linearly independent polarization states [e.g., parallel (π) and perpendicular (σ) to the scattering plane], the cross section for coherent elastic scattering is obtained from the definition²

$$\frac{d\sigma}{d\Omega} = \text{Tr}\{F_{E1}^\dagger \rho F_{E1}\}, \quad (3)$$

where ρ is a density matrix, which describes the polarization states of the incident photons, and

$$F_{E1} = \sum_n e^{i\mathbf{K} \cdot \mathbf{R}_n} f_{E1}.$$

In the last expression, n runs over all ions, \mathbf{K} is the scattering vector, and $r_0 = e^2/mc^2$. *Ab initio* calculations of the resonant-magnetic-scattering cross section for an isolated magnetic ion will be discussed in Sec. VI.

The last point worth making about the cross section is that it is sensitive to the direction of the magnetic moment through the scalar product in Eq. (1). If we use σ -polarized incident radiation (the normal polarization from a synchrotron source), the emitted resonant-magnetic scattering is rotated to π polarization. Moreover, the vector $(\hat{e}'^* \times \hat{e})$ is parallel to $\hat{\mathbf{k}}'$. In all the antiferromagnetic reflections examined in this study, $\hat{\mathbf{k}}'$ is never perpendicular to \hat{z} , so that nonzero intensities should be observed. This is different from the situation in neutron scattering for both USb and $(U_{0.85}Th_{0.15})Sb$, in which no magnetic scattering is observed along the $(00l)$ axis because the spin components are along this direction (Table I) and polarization dependence of neutron scattering varies as $\mathbf{z} \times \mathbf{K}$, so that no scattering is observed when these are parallel. We have attempted to relate the intensities for various magnetic peaks to the geometric term $(\hat{e}'^* \times \hat{e}) \cdot \hat{z}$ as is routinely done in neutron scattering to determine the direction of \hat{z} , but the varying absorption coefficients when the crystal is rotated away from the $(00l)$ direction make only qualitative comparisons possi-

ble. The general trends are, however, consistent with Eq. (1), and the moment directions are given in Table I.

B. Least-squares fit of data

As shown by the work on UAs,⁵ nonresonant-magnetic scattering is several orders of magnitude weaker than resonance scattering in the vicinity of the absorption edges of actinides, and we may safely neglect it, provided that we confine our attention to energies near the absorption edges.

Using standard formulas for atomic resonances, we may convert Eq. (2) to give the polarization amplitude as

$$f \propto i \left\{ \frac{1}{[(E_r - E)/(\Gamma/2)] - i} - \frac{1}{[(E_r + E)/(\Gamma/2)] - i} \right\}, \quad (4)$$

where we have used E_r , the resonance energy, to replace $(E_{\alpha j'} - E_{\alpha j})$. The second term is of no interest in producing the resonance, and we neglect it as a part of the background. We must now consider two resonances, M_{IV} and M_V , each with amplitudes A_4 and A_5 , widths Γ_4 and Γ_5 , and energies E_4 and E_5 , respectively. After collecting terms we find

$$I(E) \propto |f^{\Pi}|^2 \propto \left[\frac{A_4}{1 + [(E_4 - E)/(\Gamma_4/2)]^2} - \frac{A_5}{1 + [(E_5 - E)/(\Gamma_5/2)]^2} \right]^2 + \left[\frac{A_4}{1 + [(E_4 - E)/(\Gamma_4/2)]^2} \left[\frac{E_4 - E}{\Gamma_4/2} \right] + \frac{A_5}{1 + [(E_5 - E)/(\Gamma_5/2)]^2} \left[\frac{E_5 - E}{\Gamma_5/2} \right] \right]^2. \quad (5)$$

This is the form used to fit our data shown in Figs. 1–6. It is identical to that used by McWhan *et al.*⁵ in the case of UAs, except that they included a term to account for the M_{III} resonance at 4.3 keV. However, the amplitude of this term is more than an order of magnitude less than A_5 and less than 0.5% of A_4 , so that we may safely neglect it. The resulting parameters are given in Table II.

Construction interference occurs between the two resonances, as may be seen by the linear term in the second part of Eq. (5). The term $E_5 - E$ changes sign at $E = E_5$. Since the contribution from the M_{IV} resonance is still appreciable at E_5 , a sharp drop in intensity should be observed as the energy increases above this value. In the case of UO_2 , this region is complicated by the presence of the special multiple-scattering condition at 3.56 keV (see Sec. II), but the sharp falloff in intensity is seen in USB

(see Figs. 4 and 5) and $\text{U}_{0.85}\text{Th}_{0.15}\text{Sb}$ (see Fig. 5) cases.

Although we have used a least-squares program to give the results in Table II, there is strong correlation between the parameters, and so it is not possible to allow all six parameters to vary simultaneously. The figures show that the quality of the fits on both a detailed linear scale near the resonances and over the total-energy range on a logarithmic scale are good.

C. Polarization analysis

As discussed in Sec. IV A, the polarization dependence of the resonant scattering should be completely rotated $\sigma \rightarrow \pi$. We have examined this for the (001) reflection from UO_2 , and the results are shown in Fig. 6. In agreement with expectations, we find the magnetic scattering rotated from σ to π polarization. Moreover, the energy dependence of the line shapes of the total magnetic cross section and π -polarized component are identical. The small signal in the σ - σ channel is consistent with the existence of a small π -polarized component in the incident beam.

D. Search for effects at Th resonances

The absorption edges are, of course, element specific. In the pseudobinary compound $(\text{U}_{0.85}\text{Th}_{0.15})\text{Sb}$, the thorium atoms will be distributed randomly over the cation sublattice in the NaCl structure appropriate to this compound. It is known from both neutron and magnetization studies that this compound is antiferromagnetic ($T_N \sim 190$ K) with an ordered moment of $2.65\mu_B$ per uranium atom.¹⁴ The free-atom configuration of thorium is $6d^27s^2$, and in compounds it is normally tetravalent. No magnetic thorium compounds are known, and the $5f$ state in most such compounds is some 5 eV above the

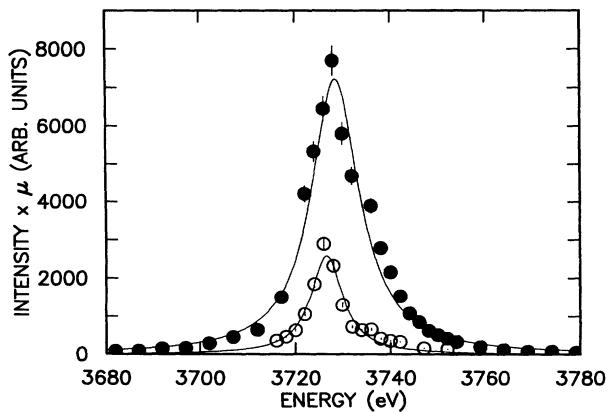


FIG. 6. Energy dependence of the $\text{UO}_2(001)$ magnetic reflection for the two polarization states: (●) σ - π and (○) σ - σ . The $\sigma \rightarrow \sigma$ counts have been multiplied by a factor of 5.

TABLE II. Parameters determined from fitting Eq. (5) to the experimental data. Figures in parentheses are estimated errors on the least significant digit. The material and Bragg reflection examined are given in the first column. The theoretical branching ratios A_4/A_5 for free-ion states of $5f^2$ and $5f^3$ are 17 and 6, respectively (see Sec. V).

	Resonant energies		Amplitudes		Energy width		Intensity ratio (M_{IV}/M_V) ^{1/2} (uncorrected data)	Branching ratio A_4/A_5 (corrected data)
	(eV)		(arb. units)		(eV)			
	E_4	E_5	A_4	A_5	Γ_4	Γ_5		
UO ₂ (001)	3727	3548	190(1)	31(2)	9.8(2)	7.7(5)	7.9(2)	6.2(4)
UO ₂ (102)	3727	3549	272(1)	39(2)	8.0(2)	8.3(4)	9.4(2)	7.0(4)
USb(001)	3726	3549	88(1)	25(2)	5.9(1)	4.6(3)	5.1(1)	3.5(3)
U _{0.85} Th _{0.15} Sb(00 $\frac{5}{2}$)	3726	3548	116(1)	32(2)	6.2(1)	5.0(3)	5.2(1)	3.6(3)

Fermi level.³ We should not, therefore, expect any density of states of $5f$ electrons at the Th site. However, the electronic structure of USb, and similar actinide pnictides, is still somewhat controversial. It is commonly accepted that the U ions are trivalent in the pnictides, i.e., U^{3+} , but that there is a large degree of hybridization between the conduction-electron ($6d$ and $7s$) and $5f$ states.¹⁵ As a consequence, some degree of spin-polarized $6d$ density might occur at the Th site in the pseudobinary compound, and such a model has been used by Frick *et al.*¹⁶ in explaining some of the anomalous features of the USb-ThSb magnetic phase diagram.

Measurements in the region of the Th M_{IV} resonance ($3d_{3/2} \rightarrow 5f_{5/2}$) at 3.49 keV showed no anomaly associated with this resonance. Unfortunately, the intensity of the $(00 \frac{5}{2})$ reflection off resonance was insufficient for us to examine either the M_{II} ($3p_{1/2} \rightarrow 6d_{3/2}$) edge at 4.83 keV or the M_{III} ($3p_{3/2} \rightarrow 6d_{5/2}$) edge at 4.05 keV. We have failed, therefore, to establish the presence of any spin polarization at the Th site, but have been able to examine only the more unlikely case of $5f$ occupation. We presently lack sufficient intensity to examine the more plausible possibility of polarized $6d$ -electron density.

V. CALCULATION

In this section we discuss atomic and crystal-field calculations of the resonant-magnetic-scattering cross section for the U^{4+} and U^{3+} ions. The atomic calculation of the spectra (full multiplet structure in intermediate coupling) was performed with Cowan's atomic Hartree-Fock and multiplet programs (with relativistic corrections).¹⁷

In the case of the U^{4+} ion, transitions from the $5f^2$ -configuration lowest state, which is $\sim 88\%$ 3H_4 , to the full multiplet $3d^9 5f^3$ were calculated. For the U^{3+} ion a similar calculation was performed by considering $5f^3$ ($\sim 84\%$ $I_{9/2}$) $\rightarrow 3d^9 5f^4$.

The cross section for the atomic calculations of $U^{4+}; 5f^2$ is shown as a dashed line in Fig. 7(a). The branching ratio is ~ 17 . This is larger than the observed values of ~ 7 in Table II. More significantly, however, the atomic calculation is known to be a poor approximation to the electronic ground-state configuration in UO₂. Crystal-field effects are important and have been measured directly by neutron inelastic scattering.¹⁸

For the U^{4+} ion a calculation in an octahedral crystal field was performed using the Cowan-Butler code.¹⁹ In O_h symmetry the $5f^2$ ground state of 3H_4 (with 88% purity) splits into Γ_1 , Γ_3 , Γ_4 , and Γ_5 states. The x-ray-exchange-scattering spectrum was obtained by considering all transitions from the Γ_5 ground state (established by neutron scattering¹⁸) to the full multiplet $3d^9 5f^3$. We have tried various values of the crystal-field potentials V_4 and V_6 , always confined to $V_4 < 0$ and $V_6 > 0$, as determined in the neutron work, and find that for $V_4 = -155$ meV and $V_6 = 60$ meV we can reproduce extremely well the experimental curves of Figs. 2(c) and 3(c). This spectrum is shown as a solid line in Fig. 7(a). The values of V_4 and V_6 , although slightly different from those of Ref. 18 of $V_4 = -125$ meV and $V_6 = 25$ meV, give the same order of levels Γ_5 , Γ_3 , Γ_4 , and Γ_1 with an energy separation of 162 meV between Γ_5 and Γ_3 (this is measured at 150 meV in the neutron experiment¹⁸). Given our experimental difficulties in determining the branching ratio, the

TABLE III. Electrostatic and exchange parameters (in eV). The F and G integrals are scaled down to 80% of their HF values (see text).

		Ground state: $3d^{10}5f^n$					Excited state: $3d^9 5f^{n+1}$				
	n	$F_{(f)}^2$	$F_{(f)}^4$	$F_{(f)}^6$	$F_{(fd)}^2$	$F_{(fd)}^4$	$G_{(fd)}^1$	$G_{(fd)}^3$	$G_{(fd)}^5$	ξ_d	ξ_f
U ⁴⁺	2	7.610									0.261
U ³⁺	3	7.081									0.235
U ⁴⁺	2	8.021	5.254	3.251	2.052	0.952	1.603	0.969	0.678	73.379	0.301
U ³⁺	3	7.537	4.904	2.975	1.886	0.870	1.466	0.886	0.619	73.381	0.275

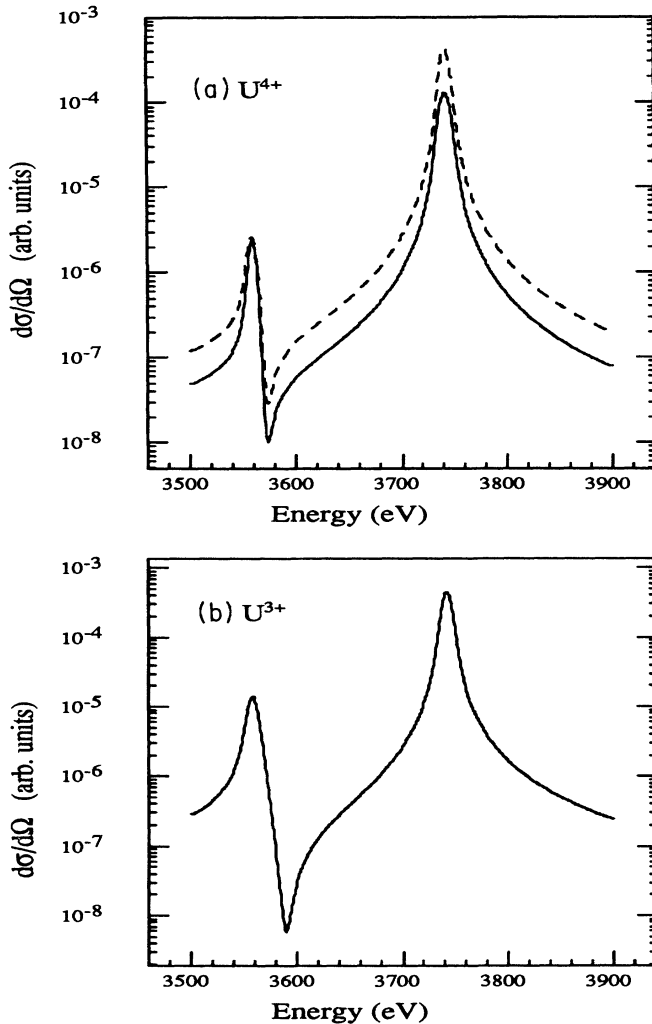


FIG. 7. Calculated resonant-magnetic-scattering cross sections for (a) U^{4+} (the dashed curve is an atomic calculation for the free-ion state, whereas the solid line includes crystal-field effects) and (b) U^{3+} ions. See text for full discussion.

agreement is clearly satisfactory. The calculations do show the sensitivity of the $5f^2$ branching ratio to crystal-field effects, which in this case reduce the branching ratio from the atomic value of 17 to ~ 7 .

In the case of the U^{3+} ion, the atomic spectrum is shown in Fig. 7(b) and gives a branching ratio of ~ 6 . A comparison with the data (Figs. 4, 5, and Table III) indicates that, within the accuracy of our experimental data, crystal-field and hybridization effects must be small. This is consistent with the fact that crystal-field transitions have not been observed in these materials with neutron inelastic scattering.²⁰

In the calculations the presence of a local magnetic moment was simulated by turning on a small external magnetic field, coupled to the ground-state spin only. The scattering amplitude was obtained by assuming a core-hole width¹¹ $\Gamma_{M_{IV}} = \Gamma_{M_V} = 4.5$ eV [full width at half maximum (FWHM)]. To reproduce the experimental widths, a further convolution with a Gaussian line shape

of standard deviation $\sigma = 3$ eV was found necessary. The electrostatic and exchange parameters F^k and G^k used in the multiplet calculations were all scaled down to 80% of their Hartree-Fock (HF) values, a standard optimization procedure in core-level spectroscopy calculations.²¹ These scaled values are listed in Table III, where the (unscaled) spin-orbit parameters $\xi_{f,d}$ are also given.

It is worth noting that in the scattering process an intermediate excitonic state is formed: In the free ions U^{n+} ($n=3,4$), the $3d$ - $5f$ Coulomb energy amounts to 27–28 eV. In the solid, screening reduces²² it to 6–8 eV, which is still larger than the $5f$ -band width. Also, we observe that in the actinides the spin-orbit interactions, relative to the corresponding Coulomb energies, are larger than in the rare earths (transitions $3d \rightarrow 4f$); the branching ratios are accordingly larger.²³

VI. DISCUSSION

We will discuss in turn the energies, widths, and amplitude ratios as given in Table II.

A. Energies of resonance peaks

The tabulated values of the M_{IV} and M_V electron-binding energies are 3728 and 3552 eV, respectively. The difference gives the spin-orbit splitting between the $3d_{3/2}$ and $3d_{5/2}$ states. For UO_2 the difference in the two absorption edges has been measured by Kalkowski *et al.*¹¹ and Guo *et al.*²⁴ as 174 eV, and Kalkowski *et al.* find that the M edges are shifted about 1.5 eV from the white-line position (defined as the inflection point of the absorption). The mean of the values in Table II gives a splitting $\Delta E = E_{M_{IV}} - E_{M_V} = 178 \pm 1$ eV, and clearly the positions are indistinguishable from the tabulated values of the electron-binding energies, for which $\Delta E = 176$ eV. Given the necessity to make large (and variable) absorption corrections at the peak positions [see Fig. 1(b)], we believe the agreement in Table II is satisfactory and that resonance-magnetic scattering from the M_{IV} and M_V absorption edges occurs at the respective electron-binding energies.

B. Energy widths

The instrumental resolution at these energies is approximately 3 eV; however, this argument is for a perfect crystal. An intrinsic crystal mosaic will effectively broaden this width, but we have not investigated this coupling in detail, e.g., by using crystals of the same material but different mosaics. Atomic calculations²⁵ suggest that $\Gamma \sim 7$ eV, and we find that the widths are very close to the atomic values. McWhan *et al.*⁵ have already discussed their unsuccessful efforts to observe exchange broadening (corresponding to a difference in energy between the up- and down-spin bands) in their data on UAs, and we have not attempted any analysis along this line. Instead, we were particularly interested to measure the widths in UO_2 because it is a semiconductor, whereas all the other materials are semimetals, with hybridized $5f$ -($6d7s$) bands.^{3,15} Because the conduction electrons

near the Fermi level in the uranium pnictides provide additional channels for the radiative decay of the excited state, the lifetime of this state in the semimetals would be expected to be shorter than in the semiconductor UO_2 . Since the lifetime is proportional to Γ^{-1} , we should expect the semiconductor to have the narrowest energy width Γ . This is not the case, but the UO_2 crystal also has the broadest mosaic, almost 5 times the very sharp mosaic of the uranium monopnictide crystals. Thus we cannot draw a definite conclusion at this time. Effects related to core-hole lifetimes will certainly be difficult to establish.

C. Branching ratios

It must be remembered in examining the experimental branching ratios in Table II that the absorption correction has not been made properly. Whereas the errors indicated accurately reflect the fitting, the branching ratios must be regarded as qualitative until direct measurements of the absorption are made through thin foils of the respective materials. Nevertheless, the calculations (Sec. V) show that for $\text{U}^{4+}:5f^2$ as in UO_2 the initial branching ratio is 17, but the inclusion of crystal-field effects, as observed in neutron scattering,¹⁹ reduces it to ~ 7 . For the primarily trivalent uranium compounds²⁶ USb and $\text{U}_{0.85}\text{Th}_{0.15}\text{Sb}$, on the other hand, neutron inelastic scattering²¹ has shown that the crystal-field interactions are smaller than in the oxides, so that we would anticipate the branching ratio to be close to the initial atomic calculation of 6. The results in Table II are qualitatively consistent with this interpretation.

VII. CONCLUSIONS

The present paper discusses resonant-magnetic x-ray scattering measured at the M edges in a series of antiferromagnetic uranium compounds. In agreement with earlier work^{5,9} on UAs and UN,²⁷ we find very large enhancements of the magnetic cross section at these energies. The magnetic scattering is rotated $\sigma \rightarrow \pi$ in polarization, in agreement with theory.

We have attempted to perform accurate fits to the experimental data to extract parameters that may reflect the electronic structure of the materials (Table II). The fits are very good and suggest that resonant scattering is well described in terms of atomic physics. The positions of the peaks are consistent with the M_{IV} and M_{V} electron-binding energies. Small differences of 1–3 eV, as seen by Kalkowski *et al.*¹¹ in the positions of the absorption edges for different materials, are beyond our experimental accuracy, primarily because of the necessity to make large energy-dependent absorption corrections. The energy widths are wider than the experimental reso-

lution (~ 3 eV), but there are no major differences in the different materials.

Although quantitative corrections for absorption, which we have not yet succeeded in performing, constitute a major experimental difficulty, the measurement of the branching ratio (A_4/A_5 in Table II) is capable of providing information on the electronic structure. It will be most interesting, for example, to measure the branching ratios in antiferromagnetic heavy fermions such as UPt_3 and URu_2Si_2 ,²⁸ where the number of $5f$ -electron states is a matter of debate.

Recently, it has been shown²⁹ that in ferromagnets the integral of the circular dichroism over a given edge is proportional to the ground-state expectation value of the orbital angular momentum operator L_z in type-I antiferromagnets, where $\langle L_z \rangle$ is determined by the integral (in our case over the M_{IV} and M_{V} edges) of the imaginary part of the x-ray-exchange-scattering forward-scattering amplitude. Our calculations for U^{4+} show a $O_3 \rightarrow O_h$ reduction of $\langle L_z \rangle$ by $\sim 40\%$. These findings should stimulate further experiments to study the quenching of the orbital momentum in actinide systems.

An initial attempt was made to see if any effects were associated with the M_{IV} resonance of Th in the pseudobinary $(\text{U}_{0.85}\text{Th}_{0.15})\text{Sb}$. None were found, but the intensity of the $(0,0,\frac{5}{2})$ reflection in this material was rather low. Further experiments at the M_{II} and M_{III} Th edges would appear to be more likely to give a positive result. Even more interesting will be experiments involving pseudobinaries of actinide elements known to possess occupied $5f$ electrons, e.g., $(\text{U,Np})\text{Te}$ compounds. We have recently established procedures to enable us to work on transuranium materials.

ACKNOWLEDGMENTS

We wish to thank M. Blume, M. S. S. Brooks, D. McWhan, J. B. Hastings, and D. P. Siddons for a number of interesting discussions, D. Jones and L. Rebersky for their help in some of the experiments, and J. Rebizant for help in preparing the UO_2 crystal. P. Carra acknowledges fruitful discussions with M. Altarelli, F. de Bergevin, and G. A. Sawatzky. The NSLS is operated as a user facility by the U.S. Department of Energy; work performed at BNL is supported by the U.S. DOE under Contract No. DE-AC01-76CH00016. The first three authors wish to thank the staff of both NSLS and the Physics Department for their hospitality during the course of these experiments. In addition, W. G. Stirling, G. H. Lander, and P. Carra are indebted to BNL for financial support. C. C. Tang and W. G. Stirling acknowledge the support of the Science and Engineering Research Council, U.K.

*Also at S.E.R.C. Daresbury Laboratory, Warrington, U.K.

†Present address: William & Mary College, Williamsburg, Virginia.

‡Also at Dept. of Chemical Physics, Materials Science Centre,

University of Groningen, Nijenborgh 16, 9747 AG Groningen, The Netherlands.

¹For a complete review and references, see D. Gibbs, G. Grubel, D. R. Harshman, E. D. Isaacs, D. B. McWhan, D. Mills, and

- C. Vettier, Phys. Rev. B **43**, 5663 (1991).
- ²M. Blume and D. Gibbs, Phys. Rev. B **37**, 1779 (1988); S. Lovesey, J. Phys. C **20**, 5625 (1987).
- ³M. S. S. Brooks, B. Johansson, and H. Skriver, in *Handbook of the Physics and Chemistry of the Actinides*, edited by A. J. Freeman and G. H. Lander (North-Holland, Amsterdam, 1984), Vol. 1, p. 153; M. S. S. Brooks, Physics **130B**, 6 (1985).
- ⁴D. Gibbs, D. R. Harshman, E. D. Isaacs, D. B. McWhan, D. Mills, and C. Vettier, Phys. Rev. Lett. **61**, 1241 (1988).
- ⁵D. B. McWhan, C. Vettier, E. D. Isaacs, G. E. Ice, D. B. Siddons, J. B. Hastings, C. Peters, and O. Vogt, Phys. Rev. B **42**, 6007 (1990).
- ⁶J. P. Hannon, G. T. Trammell, M. Blume, and D. Gibbs, Phys. Rev. Lett. **61**, 1245 (1988); **62**, 2644(E) (1989).
- ⁷C. Kao, J. B. Hastings, E. D. Johnson, D. P. Siddons, G. C. Smith, and G. A. Prinz, Phys. Rev. Lett. **65**, 373 (1990).
- ⁸C. Vettier and F. de Bergevin (unpublished).
- ⁹E. D. Isaacs, D. B. McWhan, C. Peters, G. E. Ice, D. P. Siddons, J. B. Hastings, C. Vettier, and O. Vogt, Phys. Rev. Lett. **62**, 1671 (1989).
- ¹⁰D. Gibbs, M. Blume, D. R. Harshmann, and D. B. McWhan, Rev. Sci. Instrum. **60**, 1655 (1989).
- ¹¹G. Kalkowski, G. Kaindl, W. D. Brewer, and W. Krone, Phys. Rev. B **35**, 2667 (1987).
- ¹²P. Carra, M. Altarelli, and F. de Bergevin, Phys. Rev. B **40**, 7324 (1989), and references therein.
- ¹³The separation of charge and magnetic scattering at $2q$ is obtained by varying the moment direction with a rotating external magnetic field.
- ¹⁴J. Rossat-Mignod, G. H. Lander, and P. Burlet, in *Handbook of the Physics and Chemistry of Actinides* (Ref. 3), Vol. 1, p. 415.
- ¹⁵B. R. Cooper, R. Siemann, D. Yang, P. Thayamballi, and A. Banerjee, in *Handbook of the Physics and Chemistry of Actinides* (Ref. 3), Vol. 2, p. 435; B. Reihl, N. Martensson, P. Heimann, D. E. Eastman, and O. Vogt, Phys. Rev. Lett. **46**, 1480 (1981).
- ¹⁶B. Frick, J. Schoenes, O. Vogt, and J. W. Allen, Solid State Commun. **42**, 331 (1982).
- ¹⁷R. D. Cowan, *The Theory of Atomic Structure and Spectra* (University of California Press, Berkeley, 1981).
- ¹⁸G. Amoretti, A. Blaise, R. Caciuffo, J. M. Fournier, M. T. Hutchings, R. Osborn, and A. D. Taylor, Phys. Rev. B **40**, 1856 (1989), and references therein.
- ¹⁹P. H. Butler, *Point Group Symmetry Applications—Methods and Tables* (Plenum, New York, 1981).
- ²⁰W. J. L. Buyers and T. M. Holden, in *Handbook of the Physics and Chemistry of Actinides* (Ref. 3), Vol. 2, p. 239.
- ²¹The scaling accounts for solid-state and configuration-interaction effects. See B. T. Thole, G. van der Laan, J. C. Fuggle, G. A. Sawatzky, R. C. Karnatak, and J.-M. Esteve, Phys. Rev. B **32**, 5107 (1985).
- ²²G. A. Sawatzky (private communication).
- ²³H. Ogasawara, A. Kotani, and B. T. Thole, Phys. Rev. B **44**, 2169 (1991).
- ²⁴J. Guo, D. E. Ellis, E. Alp, L. Soderholm, and G. K. Shenoy, Phys. Rev. B **39**, 6125 (1989).
- ²⁵M. H. Chen, B. Crasemann, and H. Mark, Phys. Rev. A **21**, 449 (1980).
- ²⁶G. H. Lander, M. H. Mueller, D. M. Sparlin, and O. Vogt, Phys. Rev. B **14**, 5035 (1976).
- ²⁷W. G. Stirling *et al.* (unpublished).
- ²⁸E. D. Isaacs, D. B. McWhan, R. N. Kleiman, D. J. Bishop, G. E. Ice, P. Zschak, B. D. Gaulin, T. E. Mason, J. D. Garrett, and W. J. L. Buyers, Phys. Rev. Lett. **65**, 3185 (1990). Unfortunately, there is no report in this paper of a measurement of the branching ratio.
- ²⁹B. T. Thole, P. Carra, F. Sette, and G. van der Laan, Phys. Rev. Lett. **68**, 1943 (1992).